Int. J. Solids Structures Vol. 28, No. 8, pp. 1053–1075, 1991
Printed in Great Britain.

0020–7683/91 $3.00 + .00
Pergamon Press plc

THE STRESSES IN A THERMALLY LOADED BIMATERIAL INTERFACE

M. Y. Tsai and J. Morton
Department of Engineering Science and Mechanics, Virginia Polytechnic Institute and State University, Blacksburg, VA 24061-0219, U.S.A.

(*Received* 24 *July* 1990; *in revised form* 2 *February* 1991)

Abstract—The conditions of equilibrium at a thermally loaded interface are considered in detail. A series of numerical models are presented to illustrate the nature of the stress system at the interface. These consist of two- and three-dimensional finite element case studies which show the limitations of existing approximate analytical solutions, and document the presence of very large normal stress gradients. The stress systems determined in the finite element calculations are in agreement with those of an experimental investigation which documented a change in sign of the stress normal to the interface, on either side of it, but which had insufficient resolution to detect the reversal of the stress which is needed to satisfy equilibrium. The implications of these large stress gradients are discussed in terms of problems involving laminated fiber composites and general bimaterial interfaces.

INTRODUCTION

A stress analysis of the heated bimetallic strip shown in Fig. 1 was first performed by Timoshenko (1925), who used a plane elasticity approach to predict the radius of curvature of such a strip. This model was successfully applied to the design of thermostats. Timoshenko's analysis predicted that the strip would develop a constant radius of curvature along its length, a result which is also derived from strength of materials arguments. Timoshenko himself pointed out a limitation of his analysis in that it could not account for the zero axial stress condition at the ends of the strip. Away from the ends of the strip, Timoshenko's solution is one-dimensional in y with the stresses defined by

Strip 1:

$$\frac{\sigma_{y_1}}{\sigma_T} = \frac{3mn(1+m)(y_1/c_1)+(m^3n+1)/m}{A\sqrt{n}}$$

$$\sigma_{y_1} = \tau_{x_1y_1} = 0$$

Strip 2:

$$\frac{\sigma_{x_2}}{\sigma_T} = \frac{3(1+m)(y_2/c_2)-(m^3n+1)}{A\sqrt{n}}$$

$$\sigma_{y_2} = \tau_{x_2y_2} = 0 \tag{1}$$

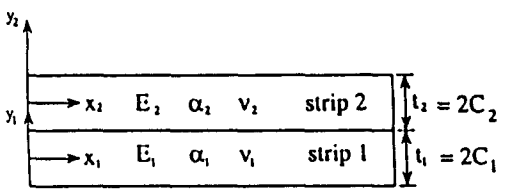

Fig. 1. General geometry of the bimetallic strip for plane elasticity analysis (Timoshenko, 1925).

where

$$m = \frac{c_1}{c_2} = \frac{t_1}{t_2}$$

$$n = E_1/E_2$$

$$A = 3(1+m)^2 + (1+mn)(m^2 + 1/mn)$$

$$\sigma_T = (\alpha_2 - \alpha_1)\sqrt{E_1 E_2}\Delta T$$

E_1 and E_2 the Young's modulus of the materials, and α_1 and α_2 the coefficients of thermal expansion. Stress components σ_{x_1}, σ_{y_1} and $\tau_{x_1y_1}$ (σ_{x_2}, σ_{y_2} and $\tau_{x_2y_2}$) are caused in Strip 1 (Strip 2) by a change of temperature ΔT.

Hess (1969) examined the stress distributions near the ends of a bimaterial interface where the shear stresses at the interface were significant. A stress field for the end loaded plate, due to Bogy (1968), was superimposed on that from Timoshenko's solution to satisfy equilibrium at the free ends. Hess showed that Timoshenko's solution was accurate provided that the length of the bimetal plate was more than twice the total depth and that the stresses were calculated no closer than at a distance equal to the total depth from the free ends.

Recently Wood *et al.* (1989) performed a detailed experimental (moire interferometry) analysis of the in-plane surface displacement fields in the interface region of a thermally loaded square steel/brass bimetal plate which had the dimensions and material properties shown in Fig. 2. The strains were obtained by taking the appropriate derivatives, and the stress components determined from Hooke's Law for plane stress conditions. The result of this was that the normal stress component perpendicular to the interface was large and tensile in the steel, and large and compressive in the brass, when the bimetal plate was cooled through 240°F. It appeared then that the conditions of equilibrium were violated across the bimaterial interface (Morton and Post, 1989).

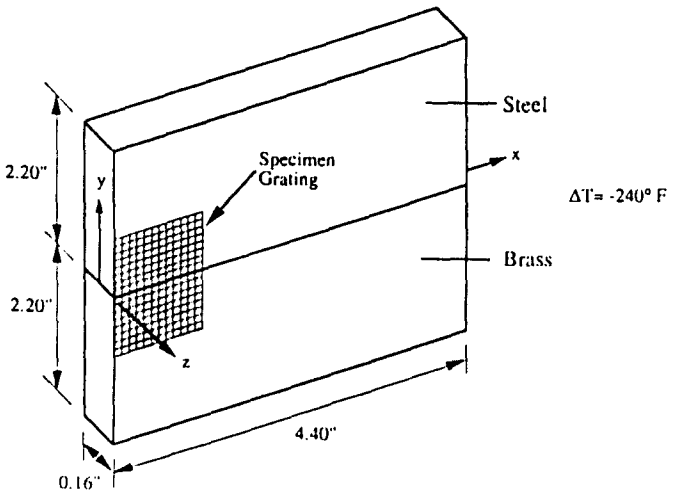

property / material	E (Msi)	ν	α (μ/°F)
Steel	29.5	0.29	6.9
Brass	15.9	0.33	10.8

Fig. 2. Plate geometry and material properties used in the moire experiment (Wood *et al.*, 1989).

The bimaterial interface has practical applications in thermostats in which the mismatch of material properties is exploited. Bimaterial interfaces are also common in the semiconductor industry where the mismatch of thermal and mechanical properties can cause severe manufacturing, service and durability problems. Parallels can also be drawn in composite technology. It is well known that laminates develop free-edge effect stresses which are not predicted by classical lamination theory but which are required for equilibrium, and which can be the cause of damage and failure in composites. On an even smaller scale, the fiber/matrix interface at a free surface would suffer from a stress system, as a result of the fabrication process or under service thermal loading, which has the same large differences in the normal stresses as the interface was approached from the fiber or the matrix.

The present study examines the mechanics of the thermally loaded bimaterial interface in detail. The apparent violation of equilibrium documented in the experimental study is investigated by considering a number of simple bimaterial case studies which can be analyzed as two- and three-dimensional problems which reflect the nature of the phenomenon, but which are more readily amenable to numerical solution than those for which the experimental data are available.

MECHANICS CONSIDERATIONS

Timoshenko's solution for the stresses in the bimetallic strip, summarized in eqn (1), predicts two linear axial stress distributions across the strip. The normal stress perpendicular to the interface is zero in this one-dimensional approach. This cannot be applied to the geometry in Fig. 2, which represents a square bimetal plate, which is outside the (two-to-one) condition determined by Hess (1969). It might be argued that Hess's two-dimensional representation would be appropriate to this problem, in which the stresses are independent of the coordinate z. However, further application of Hess's own arguments for the free body diagrams for the steel/brass plate under thermal loading suggests that the problem is three-dimensional, as shown in Fig. 3. The plane elasticity approach yields the free body diagrams in Fig. 3a, essentially those used by Hess to illustrate the need for the normal and shear stress system (σ_y, τ_{xy}) for equilibrium at the free ends. However, precisely the same arguments must be applied across the thickness of the plate, as shown in Fig. 3b. Thus there will be a skin or boundary layer near the interface in each material. This interface effect region is a zone around the interface, intersecting the free surfaces, and extending some distance within the material. In this region a three-dimensional stress system occurs, and special characteristics will be observed at an edge, where two such regions intersect. This implies that the two-dimensional analysis of Hess may be applicable to the mid-plane of the bimetal plate, but not very close to the ends. However, no matter how thin the plate, Hess's solution will not predict the stresses on the surface of the plate close to the bimaterial interface. An essentially similar effect is observed in the finite element analysis of the free-edge effect stresses at a $\pm\theta$ interface in a composite laminate (Griffin, 1988).

The implication of this is that the experiment of Wood *et al.* (1989) will be capturing this free-edge effect in a three- rather than two-dimensional problem. The central issue is then how can the experimental observation that there are large normal stresses perpendicular to the interface on either side of it be rationalized in terms of classical equilibrium considerations? A further question concerns the size of extent of the interface effect region; what scale must be considered in order to capture it? It is clear that even in the bimetallic strip there will be an interface effect region which does not influence the curvature of the strip when thermally loaded, but which may suffer from highly localized stresses which could ultimately cause failure.

If the concept of the interfacial boundary region is correct, and Wood's experimental observations are also correct, then this region must be very small and very large stress gradients must be present within this region if equilibrium conditions were to be satisfied. Thus any analysis of the problem must have sufficient resolution to capture these gradients within this region. Treatments of the free-edge effects in composites suggest that singular stresses will occur (Pipes and Pagano, 1970; Wang and Choi, 1982), so numerical models will have to have very fine meshes.

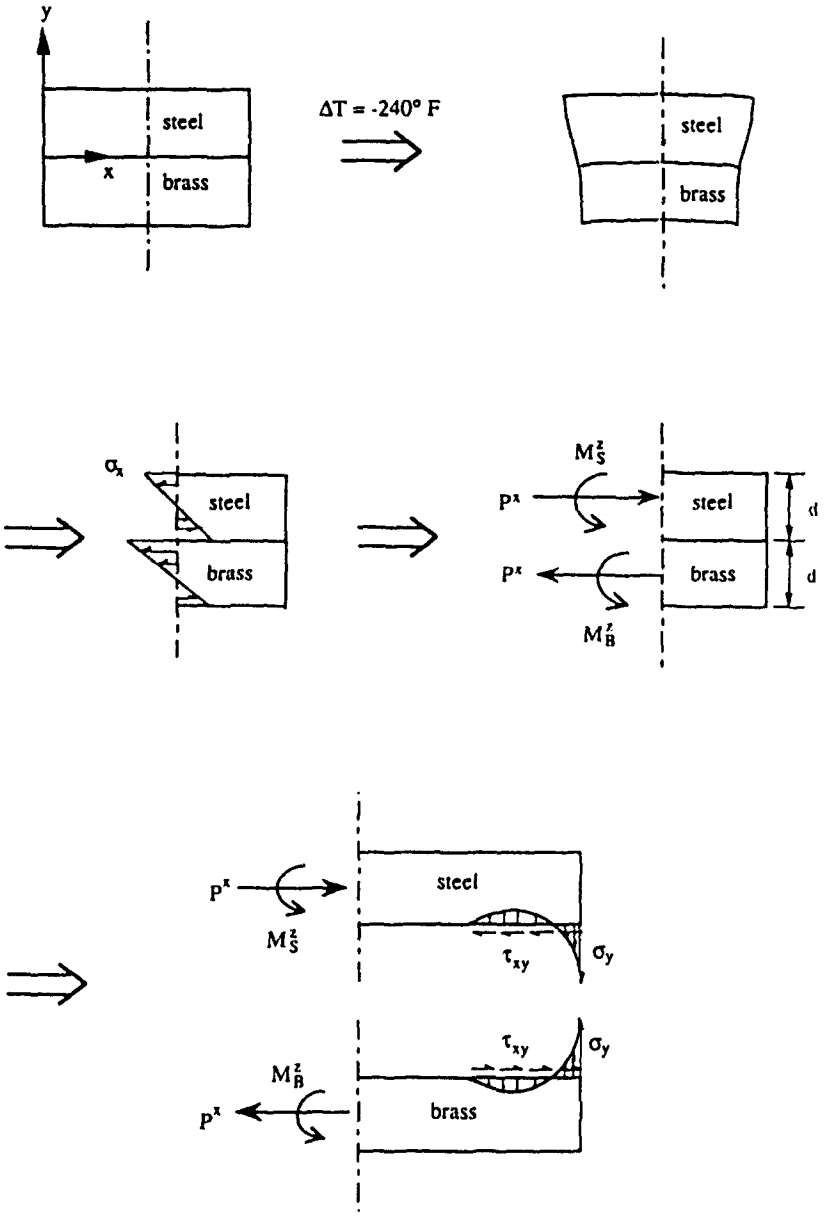

Fig. 3(a). Deformation, free body diagrams and stress systems of the thermally loaded bimetal plate in the x–y plane.

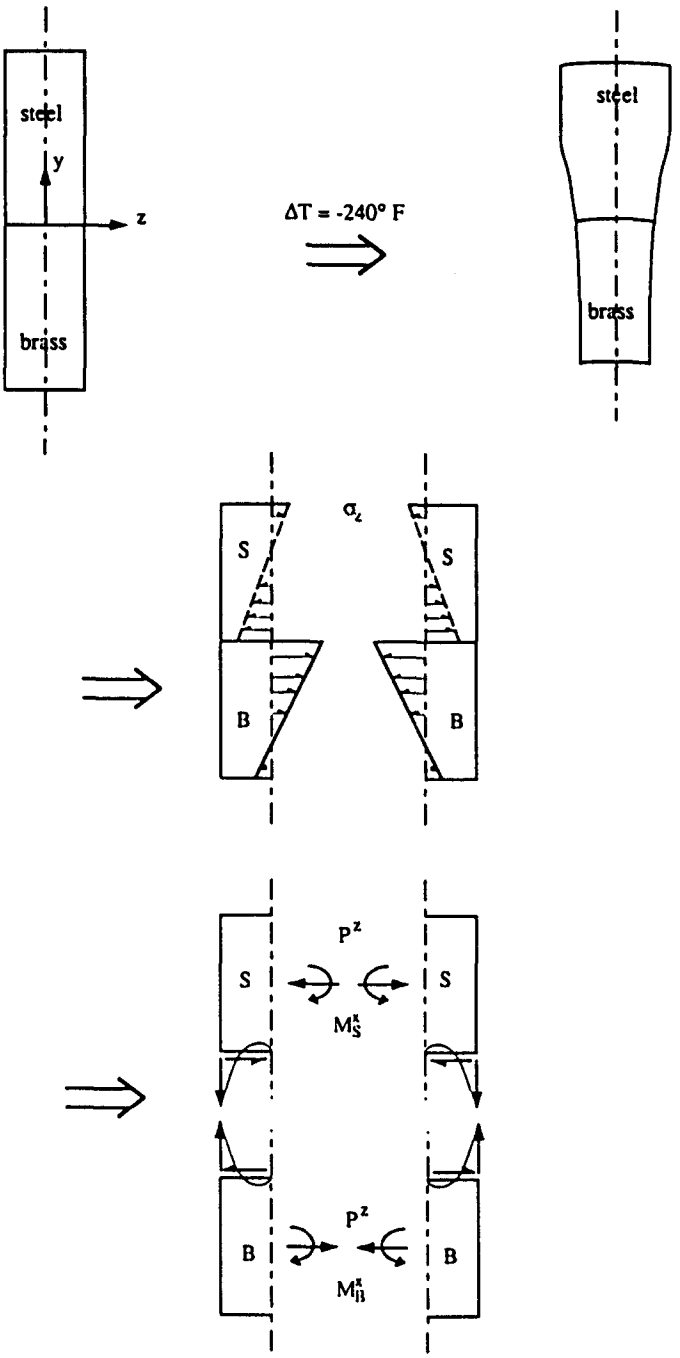

Fig. 3(b). Deformation, free body diagrams and stress systems of the thermally loaded bimetal plate in the y–z plane.

FINITE ELEMENT MODELS

Two-dimensional finite element models of Wood's bimetal plate are attractive since they can be performed with modest computational resources even for very refined meshes. Several such models are presented below in order to illustrate the limitations of two-dimensional stress analyses and the nature of the stress systems near a bimaterial interface. A two-dimensional plane stress model of the steel/brass plate is described below as the 2-D plate model, for the x–y plane in Fig. 2. Another approach is to consider the y–z plane through the middle of the plate in Fig. 2, defined by $x = 2.20$ in. It might be argued that a plane strain model could be used to investigate the stresses in this slice, near the interface, but the thermal loading precludes this. Instead, a plane stress analysis is presented below, and denoted the 2-D slice model. Rather than consider two plates, two steel/brass cylinders can be analyzed as a two-dimensional axisymmetric problem without the uncertainties of the plane stress/plane strain arguments. A bimetal cylinder is discussed below under the heading the 2-D axisymmetric model. The same mesh as the 2-D slice model can be used and the two sets of results compared with each other. In terms of the experimental data available for the steel/brass plate, the normal stresses parallel to the interface can be examined to see if the trends in the numerical models reflect the gradients needed to satisfy equilibrium while validating the experimental observations.

The plate-like geometry of Fig. 2 is not amenable to full three-dimensional analysis without recourse to substantial computational resources. To illustrate the three-dimensional nature of the bimaterial interface at an edge, two cubes with the properties of steel and brass are modeled. The model is described below under the heading the 3-D model.

All of the finite element calculations were performed on an Apollo DN 4000 workstation using the FINEL and ABAQUS codes. The analyses were linear, and used the material properties and temperature change shown in Fig. 2.

2-D plate model

The geometry shown in Fig. 4a, exploiting symmetry to produce a plate of length equal to half the length of the plate, was analyzed using four-node constant strain elements. These calculations yielded the deformed mesh shown in Fig. 4b. This deformed shape is similar

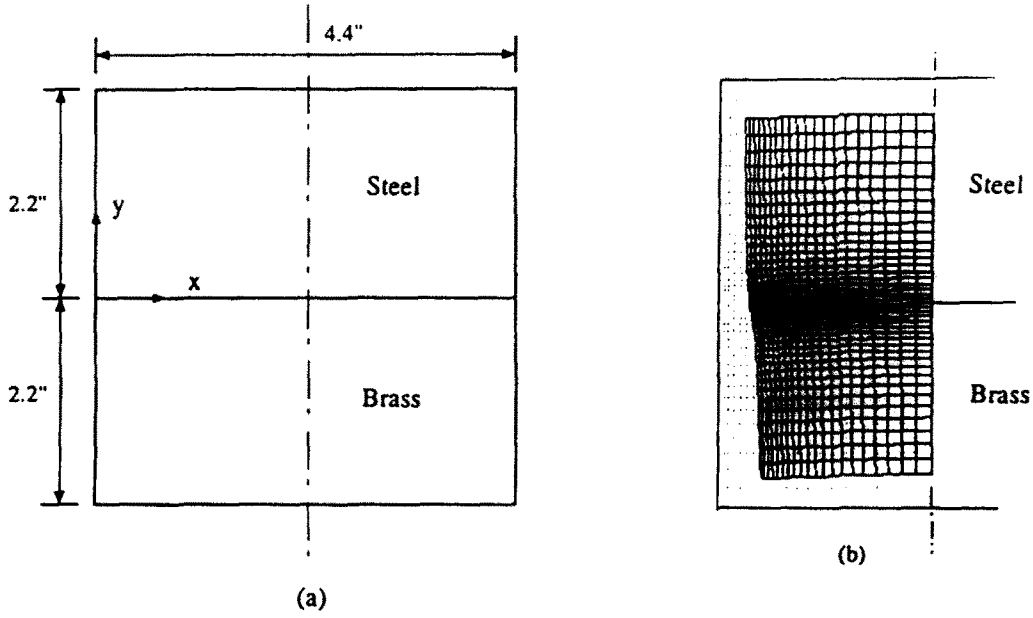

Fig. 4. Geometry (a) and deformed mesh (b) in a 2-D plate analysis of Wood *et al.* (1989) specimen. σ_x (c), σ_y (d) and τ_{xy} (e) contours in a 2-D plate analysis of Wood *et al.* (1989) specimen.

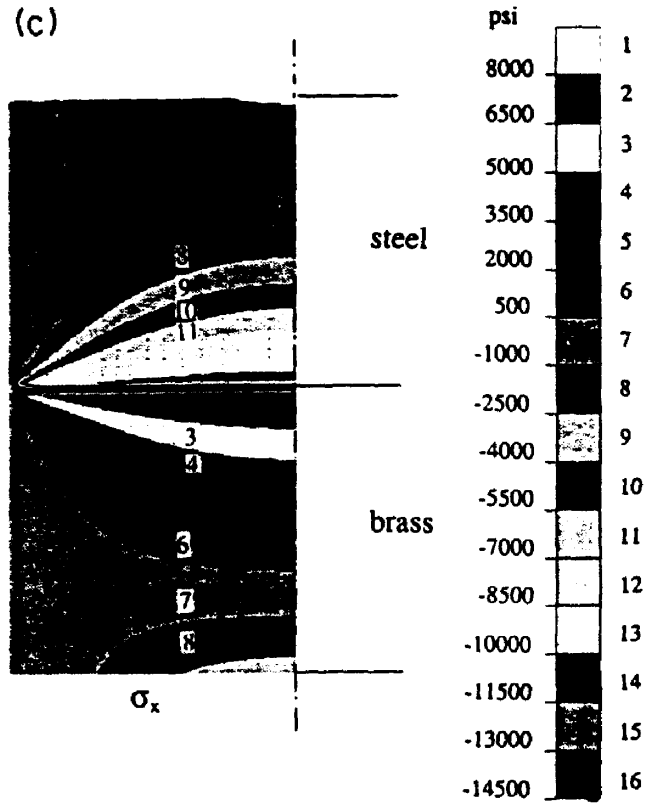

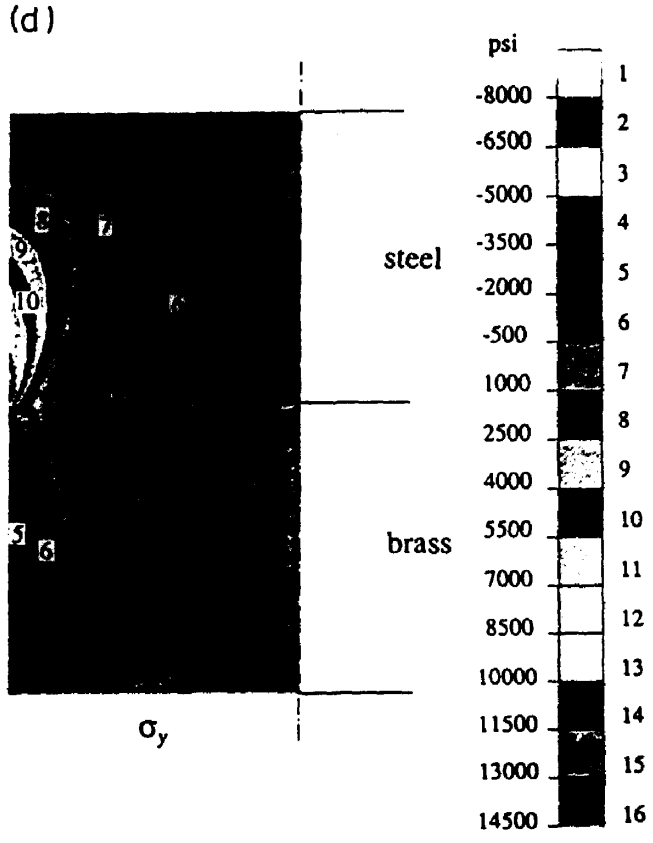

Fig. 4—*continued.*

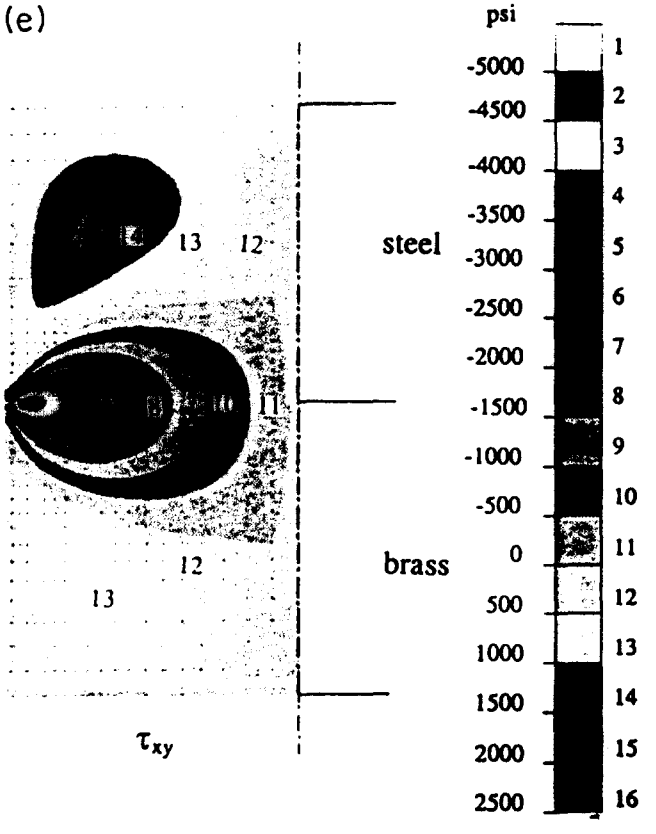

Fig. 4—*continued.*

to that used in the free body diagrams developed in Fig. 3a. Contour maps of the normal stress σ_x are shown in Fig. 4c. It is clear that at the center of the plate the stresses are almost independent of x, in agreement with Hess's observation. The contour maps of σ_y are shown in Fig. 4d. Except near the free surface, these stresses are approximately zero. A large gradient in σ_y is observed at the free surface near the interface. Along the interface shear stresses are observed, as shown in Fig. 4e, but at the middle of the plate these approach zero. Thus the two-dimensional finite element solution has all the features suggested by Hess, and even Timoshenko's assumptions are satisfied, to a reasonable degree, on a line perpendicular to the interface, through the middle of the plate. The mechanics arguments made above, however, suggest that this model will not provide an accurate assessment of the surface stresses at the interface of a real plate, even near the middle.

2-D slice model

The model shown in Fig. 5a was used, and the symmetry of the problem was exploited to produce a strip of width equal to half the thickness of the plate in Fig. 2. Eight-node

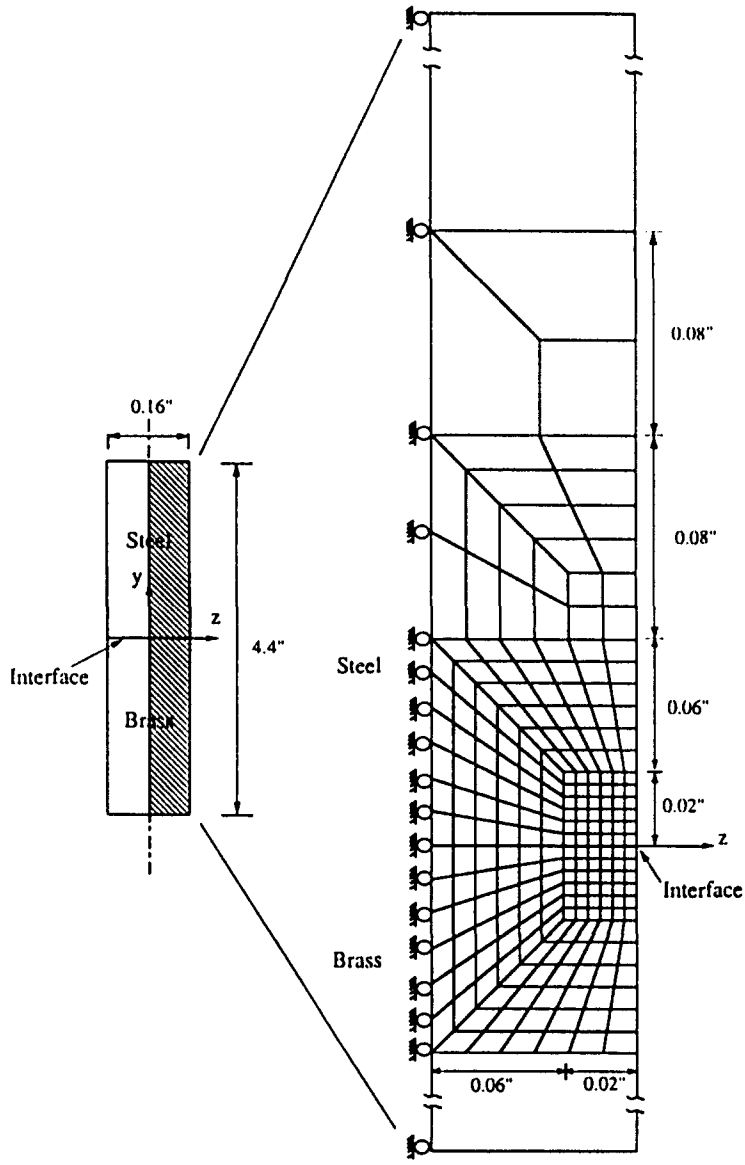

Fig. 5(a). Geometry and finite element mesh used in a 2-D slice analysis for Wood *et al.* (1989) specimen.

quadrilateral elements were employed. Note the very fine scale of the mesh in the vicinity of the bimaterial interface.

The results of the finite element computations are presented as stress distributions along four key lines defined in Fig. 5b. These consist of the line AA which corresponds to a line on the surface on either side of the interface, the lines BB and DD which are parallel and near the interface in the steel and brass respectively, and the line CC which lies along the interface. The stress components along AA are shown in Fig. 5c in which it is seen that the normal stresses σ_y on either side of the interface are indeed of opposite sign as the interface is approached, and very close to the interface the stress in the brass undergoes a very rapid reversal. The normal stress σ_z and the shear stress τ_{yz} are essentially zero, as expected from the boundary conditions, except very close to the interface; this is a finite element modeling phenomenon which will be discussed later. The stress distributions on either side of the interface (Fig. 5d, f) confirm the differences in sign in σ_y and show the

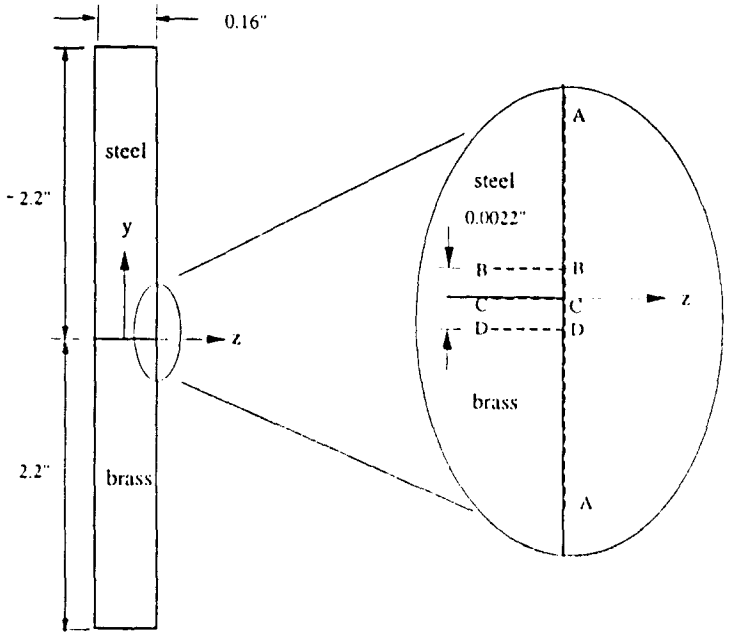

Fig. 5(b). Coordinate system and location of lines for which data are presented in the 2-D slice analysis.

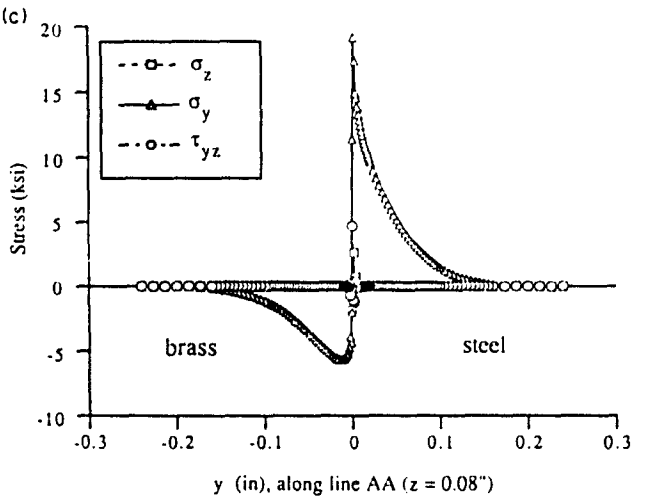

Fig. 5(c)–(f). The stress distributions along line AA (c), line BB (d), line CC (e) and line DD (f) for the 2-D slice analysis.

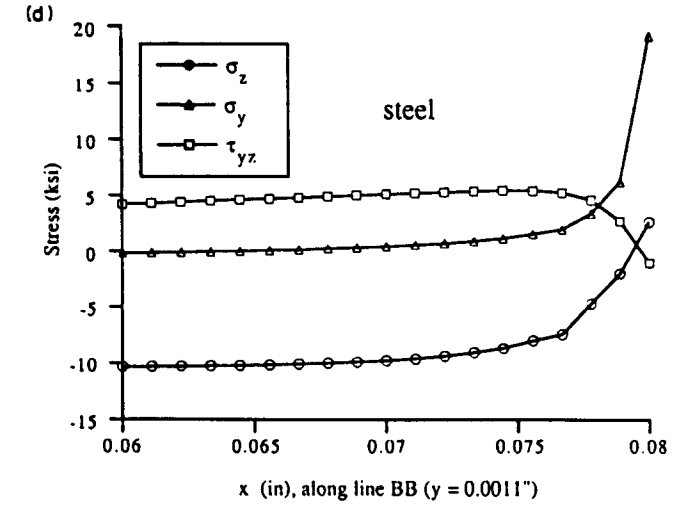

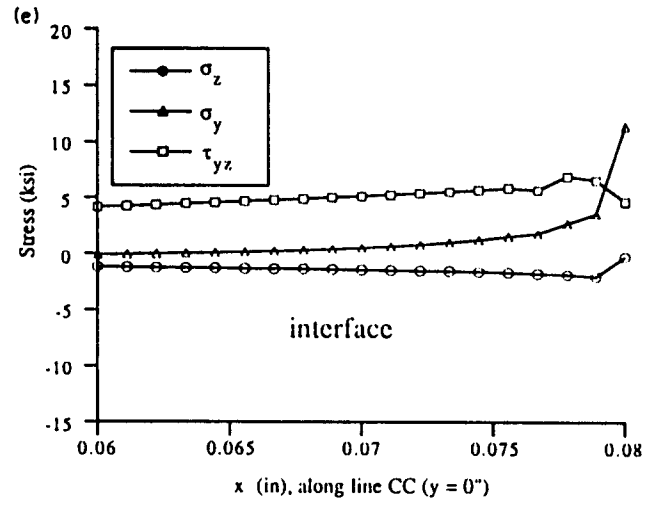

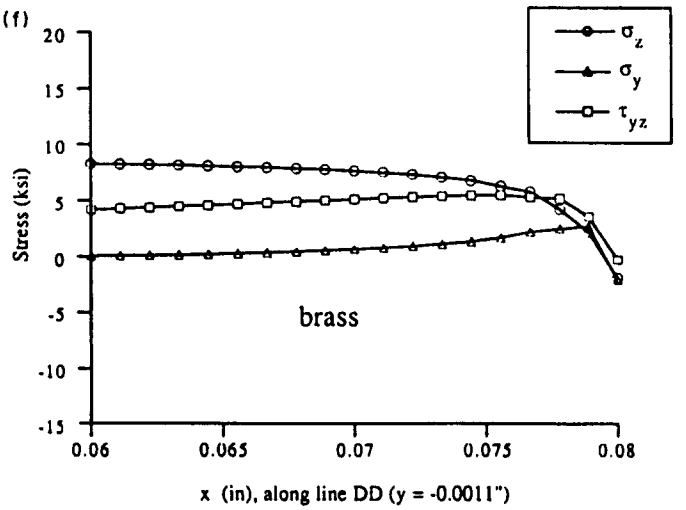

Fig. 5—*continued.*

very rapid gradient in σ_y as the surface is approached. The stresses along the interface line CC are shown in Fig. 5e, in which it is apparent that the stress σ_y is tensile at the interface on the free surface. Note that the stresses σ_z are unreliable along CC since these are discontinuous along the interface, and the calculation takes the average of these values.

2-D axisymmetric model

This model, shown in Fig. 6a, represents two solid cylinders of steel and brass. The same mesh as in the 2-D model was used but the calculation was performed with the axisymmetric option. Note that this needed a hole of small diameter to be modeled along the axis.

The stresses computed along the line AA in this model are shown in Fig. 6b. The distributions are similar in form to those of the plane stress 2-D slice case study, but the peak magnitudes of σ_y are somewhat greater. The effect of the mesh size on the stress distributions was examined by refining the mesh to yield minimum distances between nodes of a half and then a third of that in the initial mesh. The results of this convergence study are shown in Fig. 6c–e for a region very close to the interface along AA, and detailed in

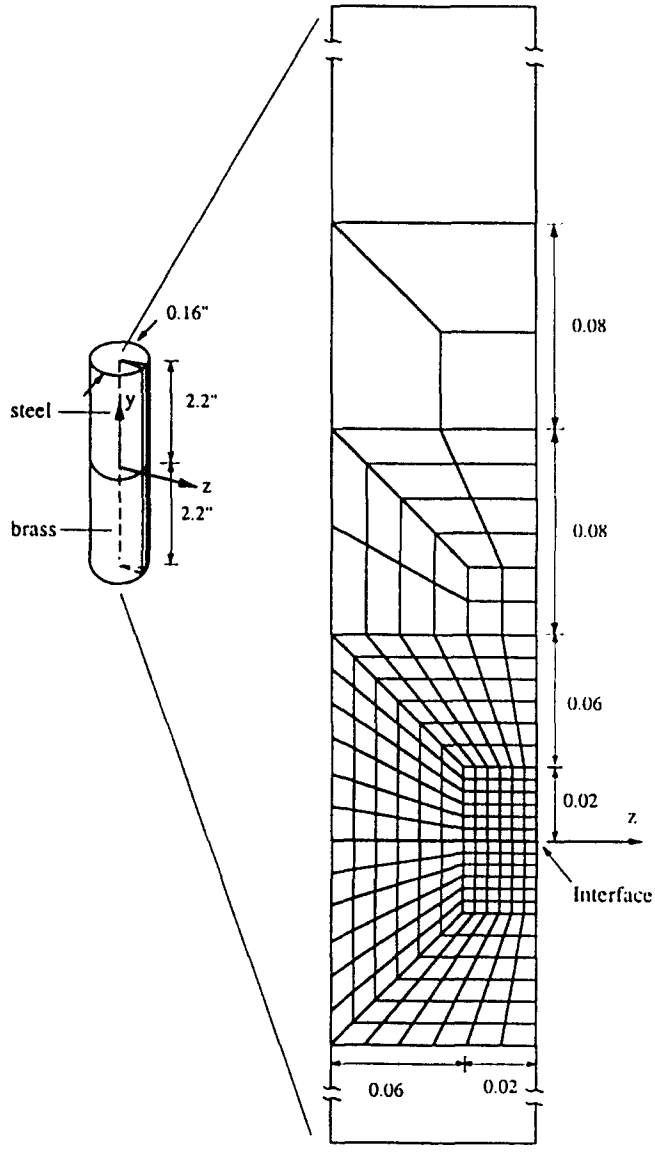

Fig. 6(a). Geometry and finite element mesh used in 2-D axisymmetric model analysis.

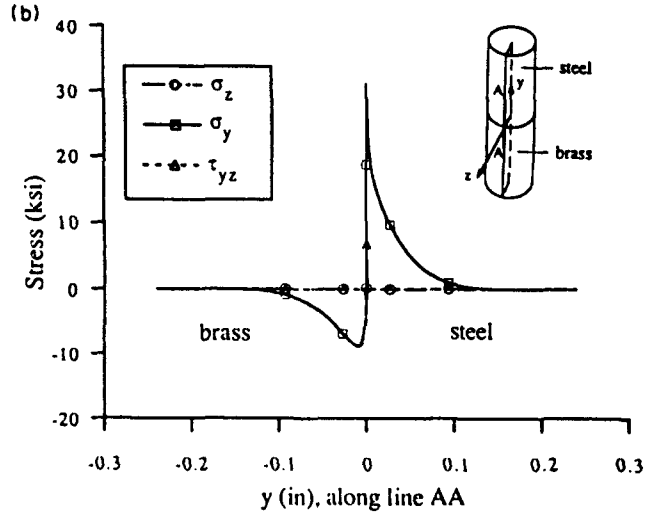

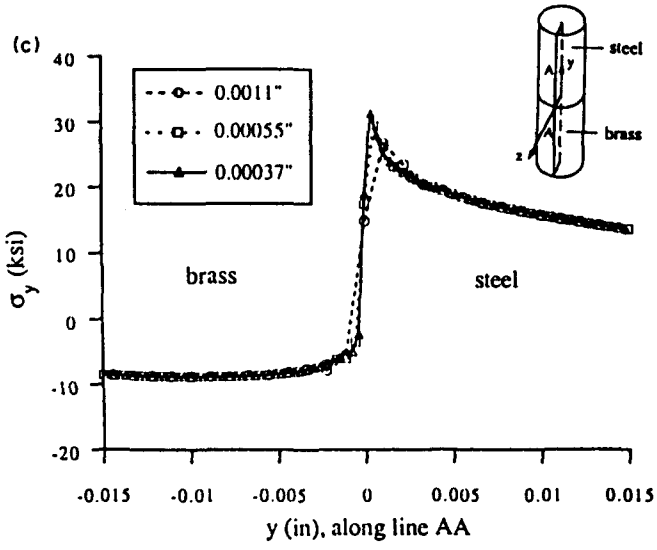

Fig. 6(b)–(e). (b) The stress distributions along line AA. (c) The normal stress σ_y, (d) the normal stress σ_z and (e) the shear stress τ_{yz} along line AA with different meshes.

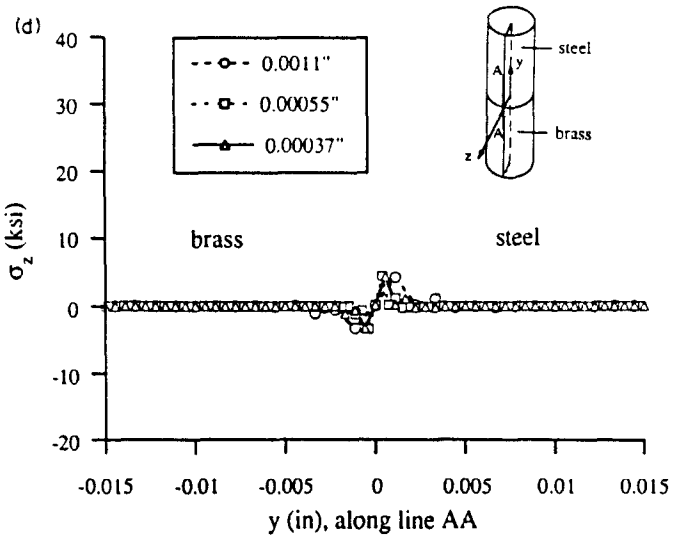

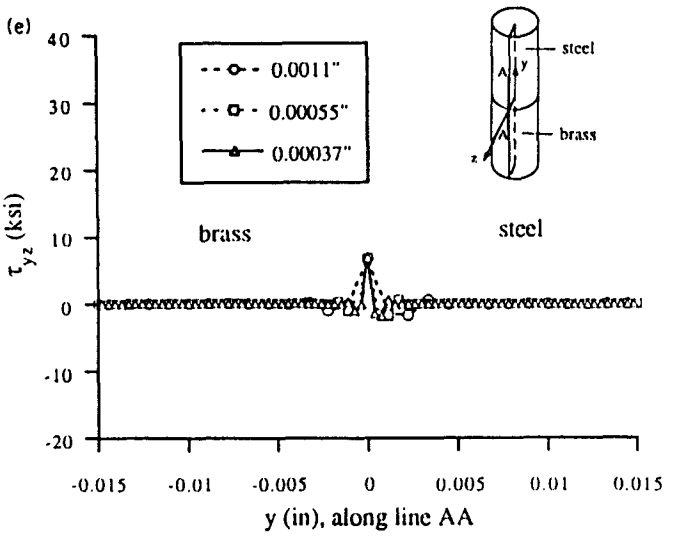

Fig. 6—*continued.*

Table 1. The results for σ_y are presented in Fig. 6c, which shows that the greatest (compressive) stress in the brass is well captured in all meshes and occurs at a distance of about 0.009 in. (or, about $0.11r$, where r is the radius of the cylinders) from the interface. As the mesh is refined the stress σ_y in the steel increases, indicating that either the mesh was not fine enough to capture a turn around in the steel similar to that in the brass but much closer to the interface, or that σ_y does not converge, but is singular. If such a stress turn around in the steel were to occur this would have to take place at a distance of less than 0.0015 in. (about $0.019r$) from the interface. The corresponding normal stress σ_z and the shear stress τ_{yz} are plotted in Fig. 6d and e, respectively. These should be zero everywhere; the non-zero values define regions in which the computations are not reliable. As the mesh is refined this zone becomes smaller so that, for the finest mesh, this represents a region of less than 0.0015 in. on either side of the interface. Within this region none of the stress component values can be used with confidence.

Table 1. Convergence study for 2-D axisymmetric model

Minimum nodal spacing (in.)	Zone of uncertainty, $\sigma_z \neq 0$, $\tau_{yz} \neq 0$ (in.)	Peak stress σ_y in steel		Peak stress σ_y in brass	
		Value (ksi)	Location (y, in.)	Value (ksi)	Location (y, in.)
0.0011	$y = -0.0044 \sim 0.0044$	19.4	0.0044	−8.8	0.0078
0.00055	$y = -0.0022 \sim 0.0022$	22.2	0.0022	−8.85	0.0094
0.00037	$y = -0.0015 \sim 0.0015$	23.8	0.0015	−8.85	0.0093

3-D model

The steel and brass cubes in Fig. 7a were modeled first with eight-node and then 20-node brick elements. The line AA in Fig. 7b represents an edge which crosses the interface. The stresses near the interface will then be affected by two interface effect zones. The normal stress σ_y along this line is shown in Fig. 7c for the eight- and 20-node element models. The peak stress values are similar to those in the cylinder case and the (compressive) stress in the brass cube also reaches its greatest value. However, the eight-node element model is not sufficient to define the location with confidence, and the 20-node element model reached the practical limits of the Apollo DN4000 workstation used in the calculations when run times of 72 h were needed. This limitation was circumvented using a two stage global–local

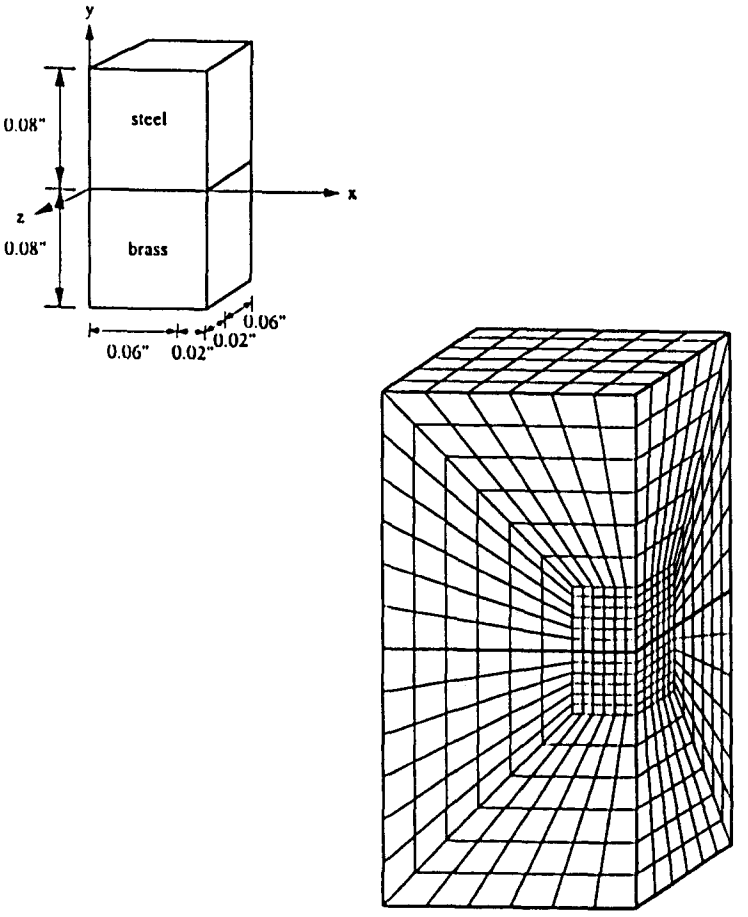

Fig. 7(a). Geometry and FEM mesh in a 3-D cube analysis.

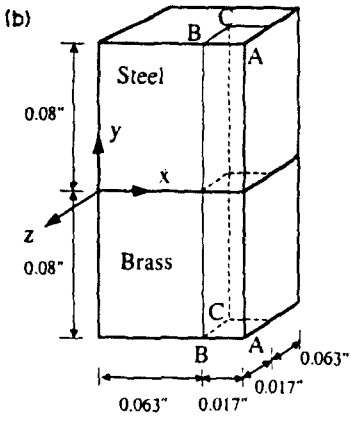

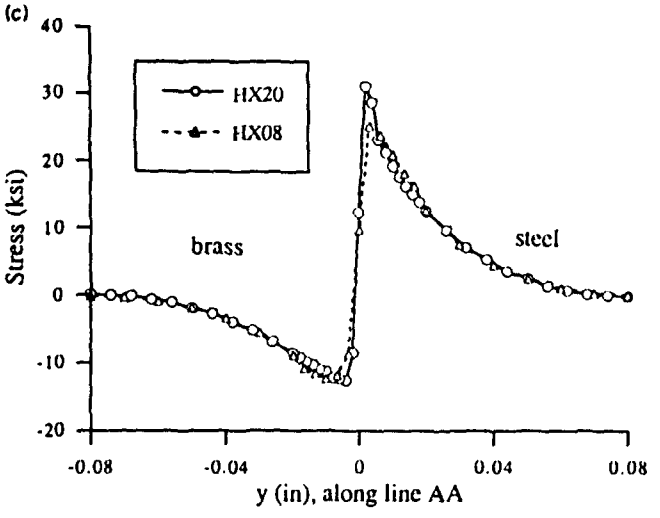

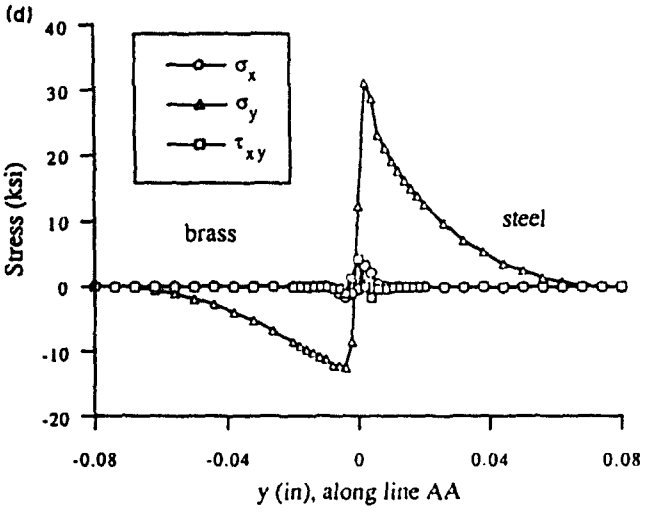

Fig. 7(b)–(f). (b) The locations of the lines AA, BB and CC. (c) The normal stress σ_y along line AA using coarse and refined meshes. The stress distributions along line AA (d), line BB (e) and line CC (f) with refined meshes are also shown.

approach (Thompson and Griffin, 1989) to show that the peak stress value and its location in the brass were reliable. The location of the peak stress in the brass occurred at about 0.004 in. (or about $L/20$, where L is the cube side) from the interface. The three stress components σ_x, σ_y and τ_{xy} are presented in Fig. 7d for the 20-node element model. Again there is a region of uncertainty on either side of the interface where the boundary conditions are not satisfied by the computed stresses. The stresses computed along the line BB, a line crossing the interface 0.017 in. from the edge, are shown in Fig. 7e. The distribution of the normal stress σ_y has a similar form to that along AA, but the peak values are lower. Note that along BB the stresses σ_x and τ_{xy} do not have to be zero everywhere. The line CC in Fig. 7b lies within the cubes and crosses the interface. The stresses σ_x, σ_y and τ_{xy} along this line are shown in Fig. 7f. Again, near the interface, the normal stress σ_y in the steel and brass is of opposite sign.

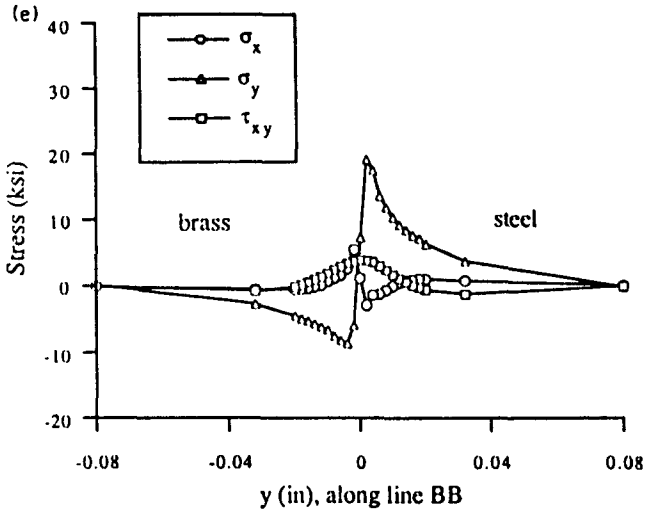

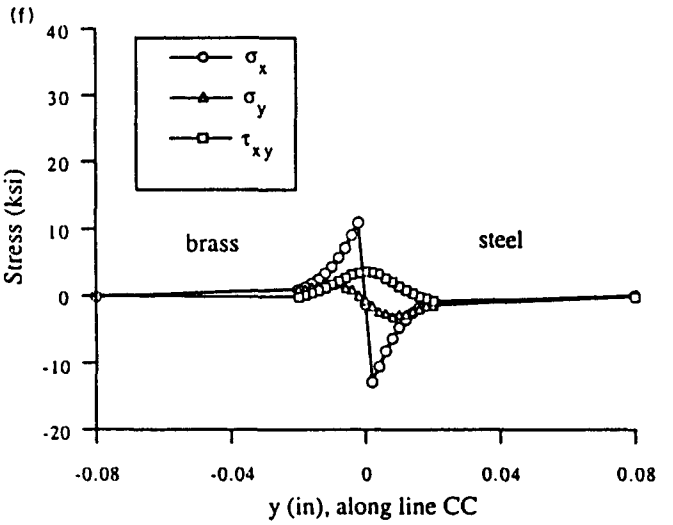

Fig. 7—*continued.*

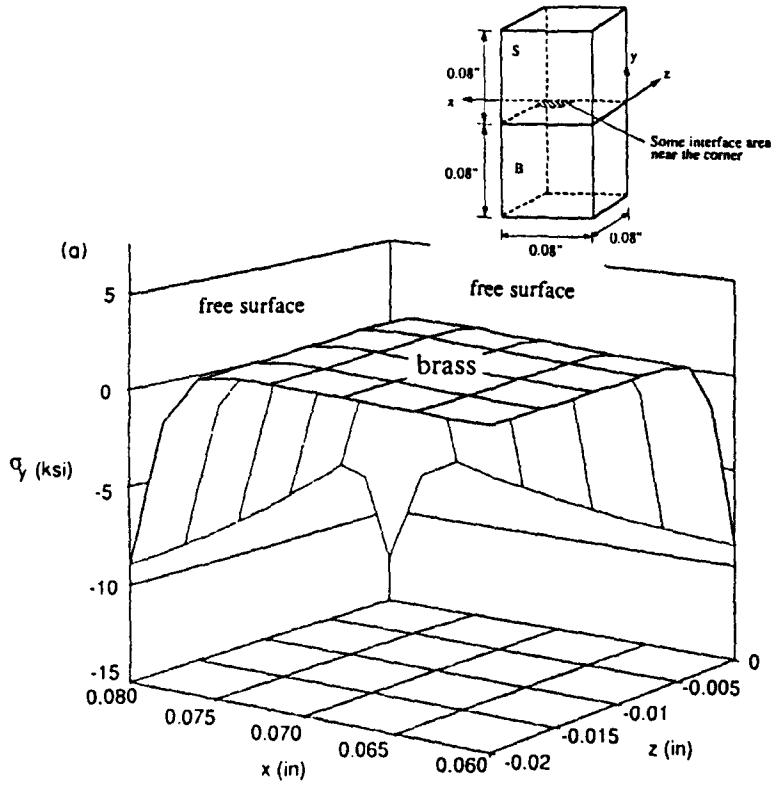
S
B
0.08"
0.08"
0.08"
0.08"
x
y
z
Some interface area near the corner
(a)
free surface
free surface
brass
σ_y (ksi)
5
0
-5
-10
-15
0.080
0.075
0.070
0.065
0.060
x (in)
0
-0.005
-0.01
-0.015
-0.02
z (in)

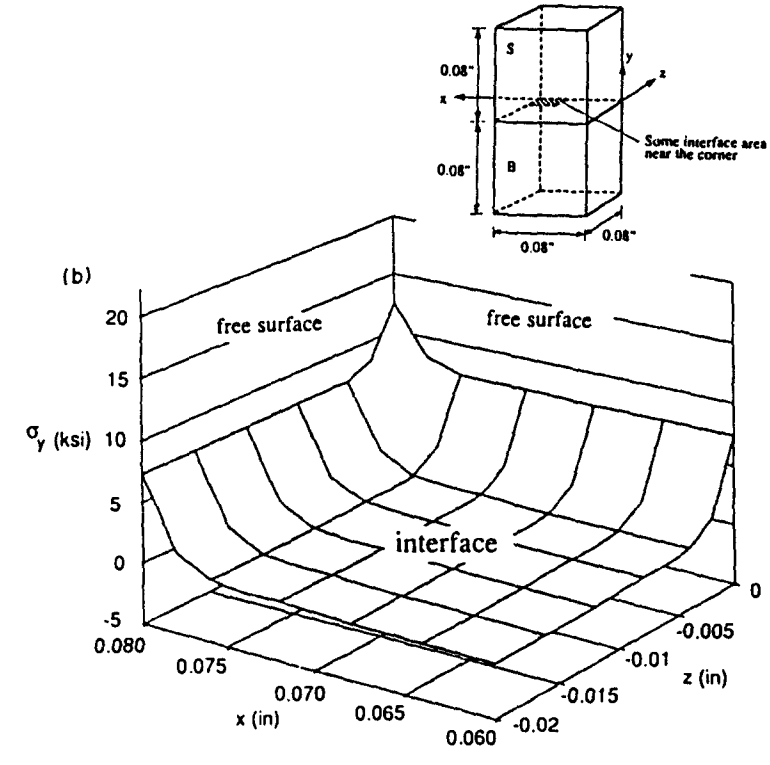
S
B
0.08"
0.08"
0.08"
0.08"
x
y
z
Some interface area near the corner
(b)
free surface
free surface
interface
σ_y (ksi)
20
15
10
5
0
-5
0.080
0.075
0.070
0.065
0.060
x (in)
0
-0.005
-0.01
-0.015
-0.02
z (in)

Fig. 8.

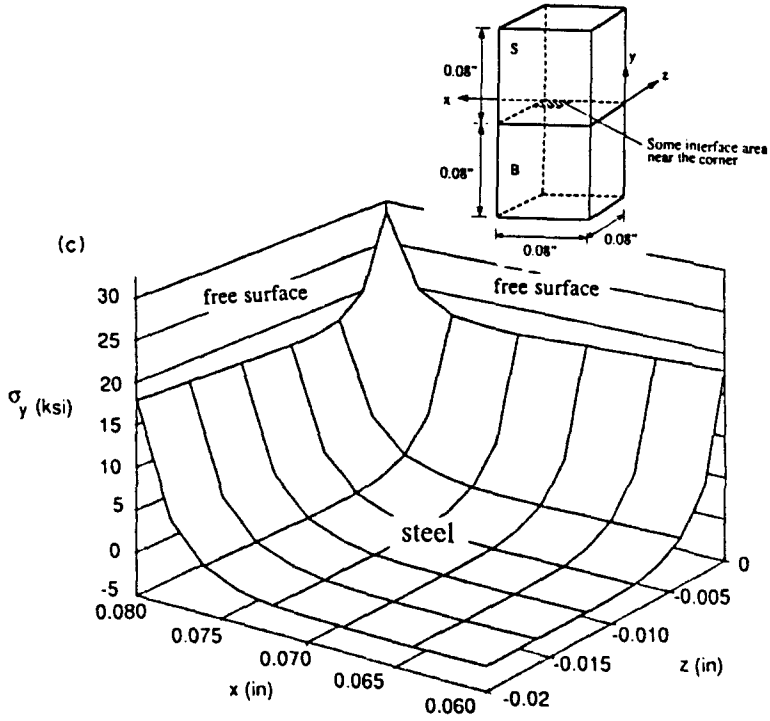

Fig. 8. The normal stress σ_y near the edge: (a) in the brass on the plane, $y = -0.004"$; (b) on the interface plane, $y = 0$; (c) in the steel on the plane, $y = 0.004"$.

Three-dimensional representations of the distribution of the normal stress σ_y can also be made. For a small region near the edge, three-dimensional plots are presented on planes 0.004 in. from the interface, in the brass, at the interface, and 0.004 in. from the interface, in the steel, in Fig. 8a–c, respectively. Compressive stresses σ_y are observed in the brass on a plane 0.004 in. from the interface, as shown in Fig. 8a. These have a value of about 8 ksi away from the edge, but reach a peak (compressive) value of about 12 ksi at the edge. The interface effect zone extends within the material about 0.004 in. to 0.008 in. (or about $L/20$ to $L/10$). The normal stress σ_y on the interface plane is shown in Fig. 8b. The stress at the free surface is tensile with a value of about 7 ksi, rising to 12 ksi at the edge. It is important to recall the limitation of the model in which the mesh is not fine enough to provide an unequivocal value of stress on the interface at the free surface. If the stress field were indeed singular, then finer meshes would simply produce larger stresses at the free surface. Very large tensile stresses are documented in Fig. 8c. These are about 18 ksi, rising to 28 ksi at the edge.

DISCUSSION

The original motivation for this study was the conflict between analytical predictions of the stresses at the bimaterial interface and those from an experiment which documented an apparent violation of equilibrium. The 2-D plate model presented above reflected all the features of Hess's analytical solution. This finite element solution is compared with Wood's experimental data in Fig. 9, in which the stress components along a line AA midway between the edge and the center of the plate are presented. It is seen that the stresses σ_x and τ_{xy} are in good agreement, but the normal stress σ_y is quite different in the analysis and experiment. The lack of agreement in σ_y strongly suggests the presence of shear stress gradients normal to the plane of the plate, and the presence of three-dimensional effects.

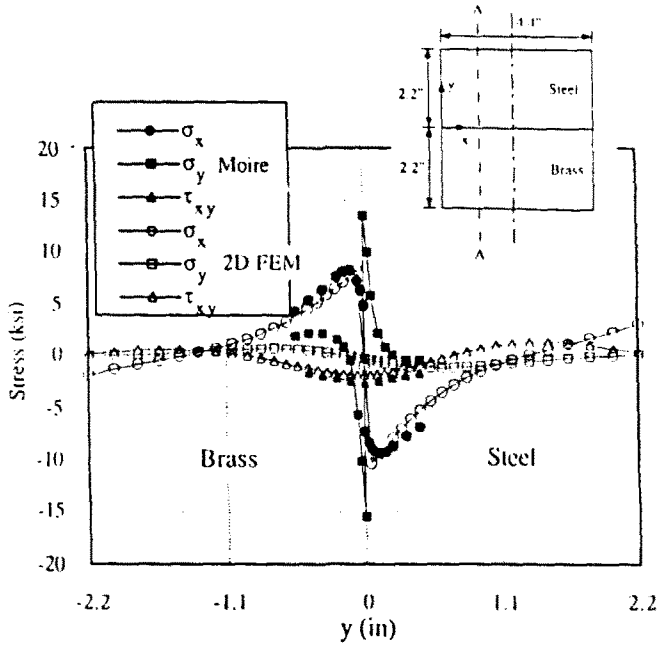

Fig. 9. A comparison of 2-D plate model and moire results (Wood *et al.*, 1989) along a line AA (midway between the edge and the center of the plate).

A comparison of the Timoshenko, moire and 2-D plate models for σ_x is shown in Fig. 10 for the same line AA. It is clear that the experiment is successful in determining σ_x so it would seem reasonable to believe that σ_y was also correct. Note also that Timoshenko's solution gives acceptable values even along this line. The equilibrium condition violation seems to be resolved in the 2-D slice and 2-D axisymmetric models. Both of these predict compressive stresses σ_y in the brass and tensile stresses in the steel, close to the interface. This agrees with Wood's experimental data. However, the numerical analyses also predict that the stress in the brass reaches a definite peak value at some location near the interface before becoming less compressive or even tensile. Both finite element models provide similar distributions of σ_y on the surface near the interface, but the peak values differ slightly, as shown in Fig. 11.

The 3-D model illustrates a phenomenon not present in the other numerical analyses, that of an edge crossing the interface. In such a region two interacting free surface effects occur, and very large normal stresses are produced. These may be singular, but practically plastic deformation or local delamination might occur. In terms of Wood's experiment, the normal stress σ_y would be distributed qualitatively as shown in Fig. 12. In this case, an experiment which measured surface parameters (displacements, strains, stresses) near the interface would document three-dimensional phenomena, no matter how thin or large the plate was. The turn around in the compressive stress in the brass seems to have occurred at a distance which was too close to the interface to be detected in Wood's experiment.

The occurrence of this interface effect region is important and well appreciated in the mechanics of laminated composites as the free edge effect. The nature of the stress gradients and stress signs of the normal stresses across such interfaces does not, however, seem to have been documented previously. The scale on which these stresses occur can have great practical significance in laminated fiber composites since these interface (free-edge) stresses may act over small distances comparable to the fiber diameter (or grain size in isotropic metals), so the continuum medium approach is limited to a scale much larger than the microstructural features. Important consequences are also apparent in the design and

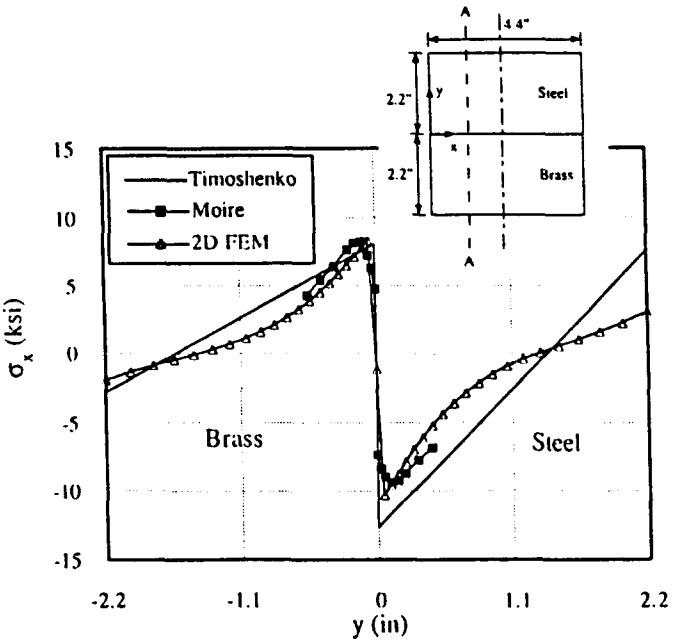

Fig. 10. A comparison of analytical, moire and finite element models for σ_x along the line AA (midway between the edge and the center of the plate).

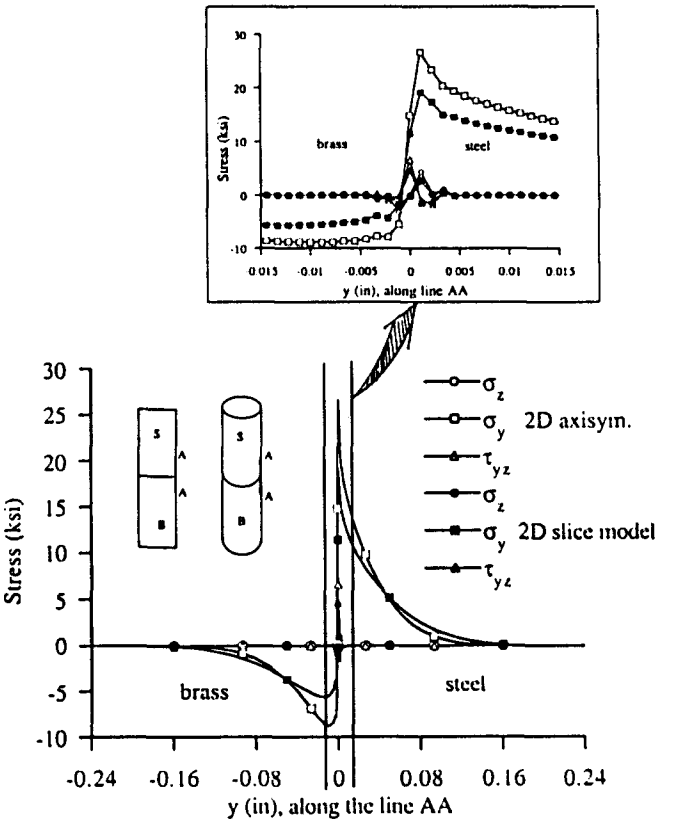

Fig. 11. A comparison of stress distributions for 2-D slice and axisymmetric models.

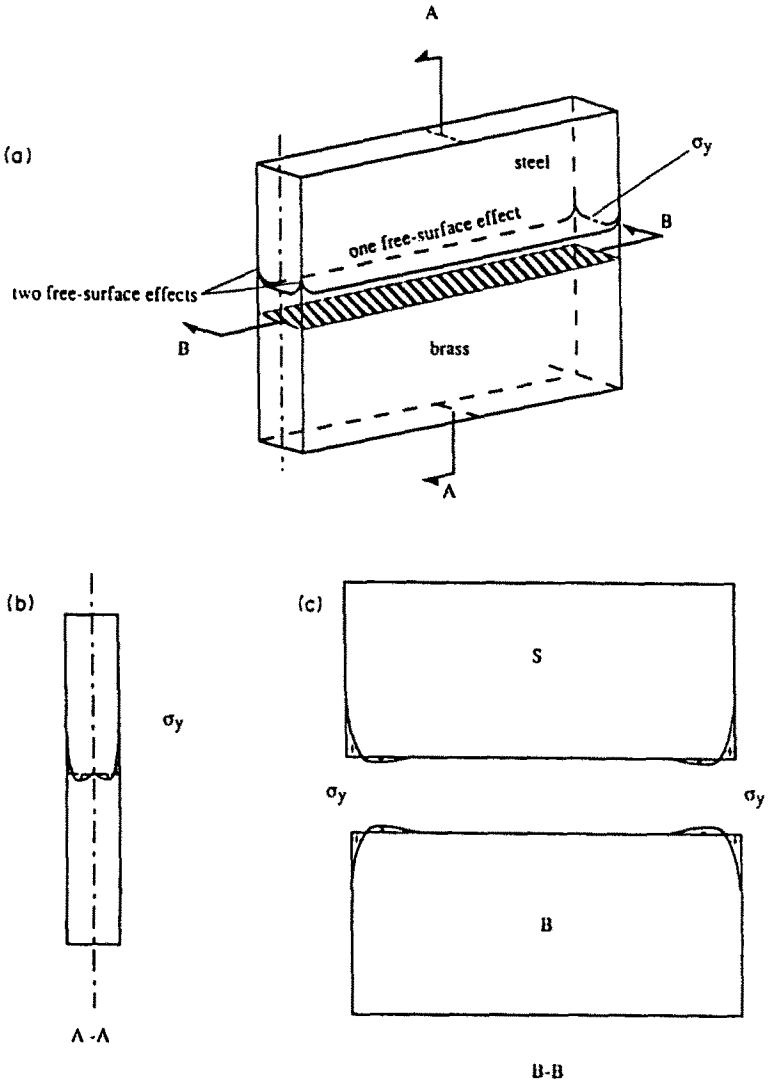

Fig. 12. Qualitative stress distribution of σ_y on the interface for plate geometry (a), for cross-section AA (b) and for cross-section BB (c).

analysis of bimaterial components of homogeneous elements. Thermal loading can produce very large normal stresses which can only be determined with three-dimensional finite element analyses with extremely fine meshes in the interface region.

CONCLUSIONS

The thermally loaded bimaterial interface suffers from a three-dimensional stress system in the vicinity of the free surface. This consists of surface stresses normal to the interface of opposite sign in each material. Very close to the interface high stress gradients occur and the stress in one of the materials, at least, will change sign to satisfy the equilibrium conditions at the interface. This boundary or skin effect will occur near the free surface and around the interface in all bimaterial problems no matter what the relative dimensions; so that in the case of the bimaterial strip model of a thermostat, for example, the one-dimensional (Timoshenko) approach would be successful in predicting the radius of curvature, and Hess's analysis would indicate the extent over which the two-dimensional shear stress system operated near the free ends of the strips, but the three-dimensional free surface effects must be incorporated in an evaluation of the largest stresses occurring in this and

related problems. The edges which cross the interface will be subjected to the largest normal stresses.

Acknowledgements—Financial support for this investigation was provided through the DARPA/BTI Program under Grant ONR/N00014-88-K-0741. Dr. Roshdy Barsoum was the contract monitor.

REFERENCES

Bogy, D. B. (1968). Edge-bonded dissimilar orthogonal wedges under normal and shear loading. *J. Appl. Mech.* **35**, 460–466.

Griffin, O. H., Jr. (1988). Three dimensional thermal stresses in angle-ply composite laminates. *J. Compos. Mater.* **22**, 53–70.

Hess, M. S. (1969). The end problem for a laminated elastic strip—Differential expansion stresses. *J. Compos. Mater.* **3**, 630–641.

Morton, J. and Post, D. (1989). Mechanics of composites: review of experiments of moire interferometry. *Proc. Am. Soc. Compos. 4th Tech. Conf.*, pp. 334–344.

Pipes, R. B. and Pagano, N. J. (1970). Interlaminar stresses in composite laminates under uniform axial extension. *J. Compos. Mater.* **4**, 538–548.

Thompson, O. M. and Griffin, O. H., Jr. (1989). 2-D to 3-D global/local finite element analysis of composite laminates. *Proc. Am. Soc. Compos., 4th Tech. Conf.*, pp. 234–237.

Timoshenko, S. (1925). Analysis of bi-metal thermostats. *J. Opt. Soc. Am.* **11**, 233–255.

Wang, S. S. and Choi, I. (1982). Boundary-layer effects in composite laminates: Part 2. Free-edge stress solutions and basic characteristics. *J. Appl. Mech.* **49**, 549–560.

Wood, J. D., Tsai, M. Y., Post, D., Morton, J., Parks, V. J. and Gerstle, F. P., Jr. (1989). Thermal strains in a bimaterial joint: experimental and numerical analysis. *Proc. 1989 SEM Spring Conf. on Experimental Mechanics*, pp. 543–551.